Available online at www.sciencedirect.com
ScienceDirect
Journal of Magnetic Resonance 188 (2007) 129–140
JMR Journal of Magnetic Resonance
www.elsevier.com/locate/jmr

^{13}C–^{13}C distance measurements in U–^{13}C, ^{15}N-labeled peptides using rotational resonance width experiment with a homogeneously broadened matching condition

Rafal Janik, Xiaohu Peng, Vladimir Ladizhansky *

Department of Physics and Biophysics Interdepartmental Group, University of Guelph, 50 Stone Road East, Guelph, Ont., Canada N1G 2W1

Received 13 April 2007; revised 6 June 2007
Available online 29 June 2007

Abstract

In this publication, we introduce a version of the rotational resonance width experiment with a homogeneously broadened matching condition. The increase in the bandwidth is achieved by the reduction of the proton decoupling power during mixing, which results in the reduction of zero-quantum relaxation, and broadens the rotational resonance condition. We show that one can achieve recoupling of the carbonyl-aliphatic side chain dipolar interactions band selectively, while avoiding the recoupling of strongly interacting C′–Cα and C′–Cβ spin pairs. The attenuation of the multi-spin effects in the presence of short zero-quantum relaxation enables a two-spin approximation to be employed for the analysis of the experimental data. The systematic error introduced by this approximation is estimated by comparing the results with a three-spin simulation. The experiment is demonstrated in [U–^{13}C,^{15}N]*N*-acetyl-L-Val-L-Leu dipeptide, where 11 distances, ranging from 2.5 to 6 Å, were measured.

Keywords: Magic angle spinning; Dipolar recoupling; Rotational resonance; Rotational resonance width; Dipolar-chemical shift correlation; Structure determination

1. Introduction

Magic angle spinning (MAS) [1] is the most commonly used method for obtaining high resolution nuclear magnetic resonance (NMR) spectra in solids. Recent studies have demonstrated the feasibility of multi-dimensional solid-state NMR (SSNMR) in samples with uniform incorporation of ^{15}N and ^{13}C labels [2–11]. Isotropic chemical shifts are available from one-, two-, and three-dimensional chemical shift correlation spectra, and provide valuable constraints on secondary structure [12,13]. More quantitative structural information is available from measurements of dipolar couplings. Dipolar interactions are averaged by MAS, but can be reintroduced through the application of amplitude and phase-modulated radio-frequency pulses. These dipolar recoupling techniques [14] have proved to be useful in applications to samples with selective incorporation of ^{13}C and/or ^{15}N labels, where accurate internuclear distance constraints could be determined [15–19]. However, application of these techniques in uniformly labeled samples is not straightforward. In particular, broadband recoupling schemes result in a continuous network of coupled spins, in which spin dynamics are generally dominated by the strongest one-bond interactions [20–22], which truncate the weak structurally constraining couplings.

Two approaches have been developed to circumvent the problem of dipolar truncation in uniformly labeled samples. In the first set of techniques it was shown that increased coupling to the proton bath, either through the reduction of the decoupling power during recoupling in proton-driven spin diffusion (PDSD), or through the active

* Corresponding author. Fax: +1 519 836 9967.
E-mail address: vladimir@physics.uoguelph.ca (V. Ladizhansky).

1090-7807/$ - see front matter © 2007 Elsevier Inc. All rights reserved.
doi:10.1016/j.jmr.2007.06.005

matching of the recoupling conditions (such as simultaneous matching of the Rotary Resonance [23] and HORROR [24] conditions in DARR experiment [25,26]) helps to restore weak dipolar interactions [27]. These approaches have recently been used for estimation of distance-constraining dipolar couplings in proteins [4,28], although the structural restraints derived from PDSD or DARR measurements are generally not accurate. Frequency selective recoupling techniques [29–33] represent the second approach to distance measurements, as they are capable of introducing only the weak couplings of interest, while the strong one- and two-bond interactions remain averaged by the magic angle spinning. The simplest to implement and perhaps the most widely employed frequency selective recoupling scheme is the rotational resonance (R^2) effect [29,34–36], which occurs when the chemical shift difference between two spins matches a small integer of the spinning frequency. The R^2 recoupling not only depends on the internuclear distance but also on the residual coupling to the proton bath, which can be described by a phenomenological zero-quantum (ZQ) relaxation rate. Despite this complication, the distances can be measured quite accurately in cases where the ZQ relaxation rate is smaller than the dipolar coupling. For example, rotational resonance has been used to measure distances in uniformly labeled amino acids and peptides [37,38], and in amyloid fibrils [39]. In the case when the ZQ relaxation rate exceeds dipolar interaction, the interpretation of rotational resonance data may result in ambiguities in the measured distances. In this respect, Costa et al. [40] have developed an alternative approach to distance measurements, which involves probing the width of the rotational resonance condition, i.e., monitoring the magnetization exchange as a function of spinning frequency, and demonstrated that both the internuclear distance and the zero-quantum relaxation rate can be extracted unambiguously from the resonance shape analysis. This Rotational Resonance Width (R^2W) method has recently been demonstrated in uniformly labeled peptides [41,42].

Selectivity of the R^2 and closely related R^2W methods is crucial for minimizing dipolar truncation and multi-spin effects. It is also a major weakness of the technique when it comes to its application to uniformly labeled proteins, as a large number of experiments are required for the measurement of the large number of distance constraints that are required to generate a high resolution structure. In general, some broadening of the recoupling resonance width would be beneficial, provided that the recoupling occurs only between weakly interacting spins. To increase the R^2 recoupling bandwidth, S. Vega and co-workers proposed a narrow-band version of radio-frequency driven recoupling [43,44], and demonstrated the utility of this technique [45,46]. In this paper, we report a different and simple way to increase resonance width of the R^2 condition—by decreasing decoupling power during mixing. The reduction of decoupling power increases residual coupling to the proton bath, broadens homogeneous width of the zero-quantum transition, and thus the recoupling bandwidth. We provide experimental evidence that this homogeneously broadened rotational resonance (HBR^2) approach can be used to accurately measure internuclear distances in uniformly labeled samples. The reduction of decoupling power during R^2 mixing, and the broadening of the R^2 width may result in the increase of multi-spin effects. We demonstrate that a simple two-spin approximation can still be used for the data analysis under the conditions of reduced ZQ relaxation, due to the attenuation of the multi-spin effects. In the extreme case, when relaxation rates are large, like in the case of proton-driven spin diffusion, the dipolar truncation effects are significantly reduced and the weak dipolar couplings are restored [27].

2. Experimental

2.1. Samples

Uniformly ^{13}C,^{15}N-labeled L-Valine, L-Threonine, L-Valine-FMOC, L-Leucine-FMOC were purchased from Cambridge Isotope Laboratories (Andover, MA). Natural abundance amino acids were purchased from Sigma Aldrich. [U–^{13}C,^{15}N]-L-Val was diluted to *c.a.* 9% in natural abundance valine, and [U–^{13}C,^{15}N]-L-Thr was diluted to 24% in natural abundance threonine. All amino acid samples were recrystallized from aqueous solution by slow evaporation at 4 °C. *N*-Acetyl-[U–^{3}C,^{15}N]-L-Val-L-Leu and natural abundance *N*-Acetyl-L-Val-L-Leu were synthesized by American Peptide. *N*-Acetyl-[U–^{3}C,^{15}N]-L-Val-L-Leu (NAcVL) was diluted to ~8% in the natural abundance NAcVL, and recrystallized from aqueous solution by slow evaporation at 4 °C as described previously [47].

In threonine, the position of Tγ resonance in the spectrum is well separated, and it can be considered a model two-spin system. Similarly, valine represents a model three-spin system, where V′ carbonyl carbon can be recoupled selectively to the side chain methyl carbons, Vγ1 and Vγ2, while V′–Vβ recoupling is suppressed. NAcVL represents a more complicated model system, where many couplings are present simultaneously.

2.2. NMR Experiments

All experiments were performed on the wide bore Bruker Avance NMR spectrometer operating at 500 MHz proton frequency. A 4 mm HXY solid-state NMR probe with X = ^{13}C was used.

The pulse sequence used in the experiments is shown in Fig. 1. In all experiments, the cross-polarization [48] mixing time was equal to 2.0 ms, with ^{1}H rf-field intensity ramped linearly around $n = 1$ Hartmann–Hahn condition [49]. The ^{1}H and ^{13}C π/2-pulse durations were 2.5 μs and 5 μs, respectively. TPPM decoupling [50] of ~79 kHz (pulse length 6 μs, with phase modulation of ±7.5°) was used during t_1 and t_2 acquisitions. CW decoupling of 100, 83, 75, 62, 50, 45, and 79 kHz TPPM decoupling were employed

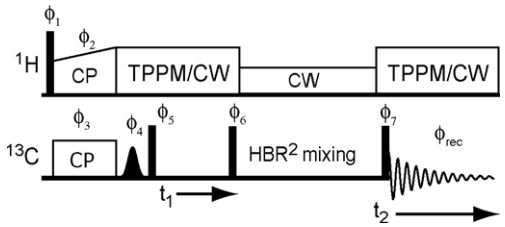

Fig. 1. A pulse sequence used to acquire 2D HBR^2 spectra in N-Ac-Val-Leu. Black rectangles denote 90° pulses. Gaussian 270° pulse is used to select carbonyl region prior to t_1 chemical shift evolution. The rest of the spectrum is suppressed by the phase cycle. The phases used in the experiments were as follows: $\phi_1 = x$; $\phi_2 = 8\times y$, $8\times(-y)$; $\phi_3 = x$; $\phi_4 = y,-y$; $\phi_5 = -y$; $\phi_6 = y,y,-y,-y$; $\phi_7 = 4\times x$, $4\times y$; $\phi_{rec} = x,-x,-x,x,y,-y,-y,y,-x,x,x,-x,-x,-y,y,y,-y$. Phase sensitive spectra in t_1 dimension were collected using TPPI scheme by incrementing the phase ϕ_6 by 90°. 1D version of the same experiment was used to collect R^2W data in threonine and valine samples.

during the R^2 mixing to control ZQ relaxation time, and to probe the dependence of the R^2 dynamics on the decoupling power.

The pulse sequence in Fig. 1 was used to study the R^2 dynamics in N-Ac-Val-Leu, where more than one carbonyl carbons are present, and multi-dimensional NMR is required to separate the R^2 recoupling occurring between different spin pairs. 1D version (no t_1 chemical shift evolution) of the same pulse sequence was used in experiments in threonine and valine.

In the experiment in Fig. 1, the selective Gaussian pulse is applied to the carbonyl region (270° flip angle, duration of 200 μs), and the phase cycle ensures that only carbonyl spins were effectively polarized prior to t_1 chemical shift evolution. The intensity of the polarization transfer to the aliphatic side chain resonances was measured as a function of the spinning frequency. In our experiments, the spinning frequency varied from 8 to 11 kHz.

The 2D spectra were processed using NMRpipe [51], and the peaks were picked and integrated using Sparky version 3 (T.D. Goddard and D.G. Kneller, University of California, San Francisco). One-dimensional spectra were processed and analyzed using Bruker XwinNMR 3.0.

2.3. Theory

2.3.1. The effective Hamiltonian

The high-field Hamiltonian for the many spin system consisting of carbonyls (I-spins) and aliphatic side chain spins (S-spins) under magic angle spinning conditions is:

$$H = \sum_i \omega_{Si}(t)S_{iz} + \sum_i \omega_{Ii}(t)I_{iz} + \sum_i \delta_{Si}S_{iz} + \sum_i \delta_{Ii}I_{iz} + \sum_{i,j} \omega_d^{(ij)}(t)\left\{2I_{iz}S_{jz} - \frac{1}{2}\left(I_i^+S_j^- + I_i^-S_j^+\right)\right\} + \sum_{i<j} 2\pi J_{ij}S_{iz}S_{jz} \quad (1)$$

δ_{Si},δ_{Ii} are isotropic chemical shifts of spins S_i, I_i. We assume that the spinning frequency approximately matches the rotational resonance condition between spins I, S, i.e., δ_{Ii}–$\delta_{Sj} \approx nv_r$, $n = 1, 2$. The dipolar interactions between these spins contribute significantly to spin dynamics and are retained, whereas the S–S and I–I dipolar interactions remain averaged by MAS, and can be neglected. The last term in the expression accounts for scalar couplings between aliphatic spins. $\omega_{Si}(t)$, and $\omega_{Ii}(t)$ represent chemical shift anisotropy of spins S_i, I_i, respectively:

$$\omega_{\lambda i}(t) = \sum_{m=-2}^{2} \omega_{\lambda i}^{(m)} e^{im\omega_r t} \quad (2)$$

$$\omega_{\lambda i}^{(m)} = \sum_{m',m''} A_{im''}^{\lambda P} D_{m''m'}^2(\Omega_{\lambda i}^{PM}) D_{m'm}^2(\Omega^{MR}) d_{m0}^2(\beta^{RL}), \quad (3)$$

where $A_{im''}^{\lambda P}$ denotes a second rank irreducible spherical tensor for spin λi ($\lambda = S,I$) in its principal axis frame. $D_{m'm}^2$, d_{m0}^2 are Wigner functions, and $\Omega^{MR} = (\alpha^{MR},\beta^{MR},\gamma^{MR})$ denotes the set of Euler angles required to transform the molecular-fixed frame M into a rotor-fixed frame R. These angles are random variables in a powder. The Euler angle is $\beta^{RL} = \tan^{-1}(\sqrt{2})$ for the exact magic angle spinning. The chemical shift anisotropy tensor of the λi spin is defined as

$$A_{i,\pm 2}^{\lambda P} = -\frac{1}{\sqrt{6}}\eta_{\lambda i}\omega_{\lambda i}^a,$$
$$A_{i,\pm 1}^{\lambda P} = 0, \quad (4a)$$
$$A_{i,0}^{\lambda P} = \omega_{\lambda i}^a,$$

where the anisotropy and asymmetry parameters are

$$\omega_{\lambda i}^a = \omega_0(\delta_{\lambda i}^{zz} - \delta_{\lambda i}^{iso}), \quad (4b)$$

$$\eta_{\lambda i} = \frac{\delta_{\lambda i}^{yy} - \delta_{\lambda i}^{xx}}{(\delta_{\lambda i}^{zz} - \delta_{\lambda i}^{iso})}. \quad (4c)$$

ω_0 in Eq. (4b) and Eq. (4c) is the Larmor frequency, $\delta_{\lambda i}^{iso} = (\delta_{\lambda i}^{xx} + \delta_{\lambda i}^{yy} + \delta_{\lambda i}^{zz})/3$ is the isotropic chemical shift. We assume that $\delta_{\lambda i}^{zz}$ is the eigenvalue of the chemical shift tensor that is the farthest from $\delta_{\lambda i}^{iso}$. Similarly, the dipolar interaction $\omega_d^{(ij)}(t)$ can also be written as a Fourier series

$$\omega_d^{(ij)}(t) = \sum_{m=-2}^{2} \omega_{ij}^{(m)} e^{im\omega_r t} \quad (5a)$$

with Fourier components defined as

$$\omega_{ij}^{(m)} = b_{ij} \sum_{m'=-2}^{2} D_{0m'}^2(\Omega_{ij}^{PM}) D_{m'm}^2(\Omega^{MR}) d_{m0}^2(\beta^{RL}). \quad (5b)$$

The through space dipolar coupling constant b_{ij} is given by

$$b_{ij} = -\left(\frac{\mu_0}{4\pi}\right)\gamma^2\hbar\frac{1}{r_{ij}^3}. \quad (5c)$$

2.3.2. Two-spin system

In the case of an I_i–S_j spin pair, the effective Hamiltonian near $n = 2$ rotational resonance condition (δ_{Ii}-$\delta_{Sj} \approx 2v_r$) can be written as [41,52]

$$H_{eff} = \Delta_{Ii}I_{iz} + \Delta_{Sj}S_{jz} + B_{ij}(I_i^+S_j^- + I_i^-S_j^+) \quad (6)$$

where the terms $\Delta_{Ii} = \delta_{Ii} - \nu_r$, $\Delta_{Sj} = \delta_{Sj} + \nu_r$ account for the off-resonance effects, and the effective dipolar interaction is given as [52]

$$B_{ij} = \left| \frac{1}{2} \sum_{m=-2}^{2} \omega_{ij}^{(m)} a_{\Delta}^{(ij,m-2)^*} \right| \tag{7}$$

with

$$\exp\{\mathrm{i}\Phi_{\Delta}^{(ij)}(t)\} = \sum_{k=-\infty}^{\infty} a_{\Delta}^{(ij,k)} \mathrm{e}^{\mathrm{i}k\omega_r t}, \tag{8}$$

$$\Phi_{\Delta}^{(ij)}(t) = \int_0^t (\omega_{Ii}(t') - \omega_{Sj}(t'))\mathrm{d}t'. \tag{9}$$

In addition to the coherent interactions approximately described by the Hamiltonian in Eq. (6), the spin system is subjected to various relaxation processes, accommodated in the Master Equation expressed in the Liouvillian space [53]:

$$\frac{\mathrm{d}}{\mathrm{d}t}\rho(t) = \hat{L}\rho(t). \tag{10}$$

The Liouville superoperator is defined as $\hat{L} = -\mathrm{i}\hat{H}_{\mathrm{eff}} - \hat{\Gamma}$. The matrix elements of the Hamiltonian commutation superoperator $\hat{H}_{\mathrm{eff}}$, and the diagonal relaxation superoperator Γ in a basis set of operators $|Q_i)$, are orthonormal in the sense that $\mathrm{Tr}(Q_i^+ Q_j) = \delta_{ij}$, and are defined as

$$(Q_i|\hat{H}_{\mathrm{eff}}|Q_j) = \mathrm{Tr}\{Q_i^+[H_{\mathrm{eff}}, Q_j]\},$$
$$(Q_i|\hat{\Gamma}|Q_j) = \frac{\delta_{ij}}{T_i}. \tag{11}$$

The parameters T_i denote relaxation times associated with the decay of coherences Q_i. The use of the diagonal representation of the relaxation superoperator is a model assumption, and implies that the decays of the multiple-quantum coherences and of the longitudinal magnetizations in the tilted frame are exponential, and that the relaxation processes of various coherences are not correlated.

For a two-spin system, Eq. (10) can be rewritten as a system of four homogeneous differential equations. We define this system in the subspace spanned by four orthonormal states $|Q_i)$, where Q_i denote spin operators

$$Q_1 = I_{iz}, \quad Q_2 = S_{jz},$$
$$Q_3 = \frac{1}{\sqrt{2}}(I_i^+ S_j^- + I_i^- S_j^+), \tag{12}$$
$$Q_4 = \frac{-i}{\sqrt{2}}(I_i^+ S_j^- - I_i^- S_j^+)$$

In this basis, the diagonal relaxation parameters for states $|Q_1),|Q_2)$ have a physical meaning of $T_1^{(1)}, T_1^{(2)}$ longitudinal relaxation times for spin 1 and 2, respectively. These relaxation times are long compared to the time scale of R^2 mixing (<50 ms), and are not going to affect the spin dynamics significantly. Thus, they will be neglected in further discussion. The diagonal relaxation parameters for states $|Q_3),|Q_4)$ are a ZQ relaxation rate $R = 1/T_2^{\mathrm{ZQ}}$. Four equations of motion for the expectation values of the operators in Eq. (12) in the vicinity of $n = 2$ ZQ resonance condition can be written as

$$\frac{\mathrm{d}}{\mathrm{d}t}\begin{pmatrix} \langle Q_1(t)\rangle \\ \langle Q_2(t)\rangle \\ \langle Q_3(t)\rangle \\ \langle Q_4(t)\rangle \end{pmatrix} = \begin{pmatrix} 0 & & & \sqrt{2}B_{ij} \\ & 0 & & -\sqrt{2}B_{ij} \\ & & -R & -(\Delta_{Ii} - \Delta_{Sj}) \\ -\sqrt{2}B_{ij} & \sqrt{2}B_{ij} & (\Delta_{Ii} - \Delta_{Sj}) & -R \end{pmatrix} \begin{pmatrix} \langle Q_1(t)\rangle \\ \langle Q_2(t)\rangle \\ \langle Q_3(t)\rangle \\ \langle Q_4(t)\rangle \end{pmatrix}. \tag{13}$$

2.3.3. Steady-state approximation

In the experimental situation of low decoupling power and short ZQ relaxation times, simple analytical solutions to Eq. (13) can be obtained for long mixing times. We will first consider an initial condition of $\langle Q_1(0)\rangle = 1$, $\langle Q_2(0)\rangle = \langle Q_3(0)\rangle = \langle Q_4(0)\rangle = 0$, as observed in 2D ^{13}C–^{13}C multidimensional experiments. Q_1 corresponds to the observable spin operator contributing to the diagonal peak, while Q_2 is the observable spin operator resulting in the cross-peak. Let us first assume that the coherences Q_3, Q_4 reach a steady state, and we can assume $|\mathrm{d}Q_{3,4}/\mathrm{d}t| \approx 0$. Under the steady-state assumption, the system of Eq. (13) can be solved analytically, and yields simple expressions for $\langle Q_1(t)$, $\langle Q_2(t)\rangle$ and $\langle Q_4(t)\rangle$:

$$\langle Q_1(t)\rangle = \langle I_{iz}(t)\rangle = \frac{1}{2}(1 + \mathrm{e}^{-2\Omega t}) \tag{14a}$$

$$\langle Q_2(t)\rangle = \langle S_{jz}(t)\rangle = \frac{1}{2}(1 - \mathrm{e}^{-2\Omega t}) \tag{14b}$$

$$\langle Q_4(t)\rangle = \frac{-\Omega}{\sqrt{2}B_{ij}}\mathrm{e}^{-2\Omega t} \tag{15}$$

where

$$\Omega = \frac{2B_{ij}^2 R}{(\Delta^2 + R^2)}, \tag{16}$$

and $\Delta = \Delta_{Ii} - \Delta_{Sj} = \delta_{Ii} - \delta_{Sj} - 2\nu_r$ measures the deviation from the exact $n = 2$ rotational resonance condition. The validity of this approximation is demonstrated in Fig. 2, where we compare the analytical solutions for $\langle Q_2(t)\rangle$ and $\langle Q_4(t)\rangle$, obtained using Eqs. (14) and (15) with the exact numerical integration of Eq. (13). For the practically important cases of structurally constraining carbonyl-side chain interactions (i.e., $\geqslant$3 bonds) the shortest geometrically allowed distance is ~3 Å, and is even longer in most other situations. Furthermore, the band selective R^2 experiments are conducted under reduced decoupling power, thus facilitating large relaxation rates. Fig. 2a compares the exact and approximate solutions for $\langle Q_2\rangle$ and $|\langle Q_4\rangle|$ for a spin pair at 3 Å apart, and a ZQ relaxation time of 1 ms. The expectation value for $|\langle Q_4\rangle|$ grows rapidly initially, and during this period, the steady-state approximation is not strictly applicable. Accordingly, the analytical buildup curve for $\langle Q_2\rangle$ deviates from the exact solution of Eq. (13) over this time period. Once the steady state is achieved, the agreement between the two solutions improves substantially. In particular, at timescales of 20 ms or longer, relevant for the R^2W experiment, the analytical

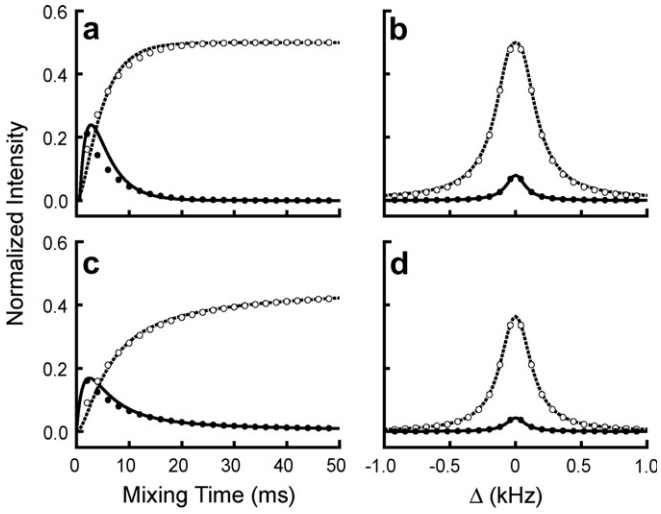

Fig. 2. A comparison of the analytical solutions of Eqs. (14) and (15) for $\langle Q_2(t)\rangle$ and $|\langle Q_4(t)\rangle|$ with the exact numerical integration of Eq. (13). In (a) and (c) the exact $n = 2$ rotational resonance condition is assumed for two spins 3 Å apart, and with $T_2^{ZQ} = 1$ ms. In (a), the results for a single orientation ($\beta = 90°$) are shown. Open and solid circles represent analytical solutions for $\langle Q_2(t)\rangle$ and $|\langle Q_4(t)\rangle|$, respectively, and solid lines show the exact solution obtained by solving Eq. (13). In (c), powder averages of $\langle Q_2(t)\rangle$ and $|\langle Q_4(t)\rangle|$ are shown. In (b), the R^2W calculations for single orientation ($\beta = 90°$) are shown as a function of the deviation from the exact R^2 condition $\Delta = \delta - 2\nu_r$, for two spins at a distance of 3 Å (open circles) and 5 Å (solid circles). Dashed and solid curves show the results of numerical solutions of Eq. (13). R^2W mixing time was 20 ms, and $T_2^{ZQ} = 1$ ms. In (d), powder averages of signals under the same conditions as signals in (b) are shown.

and the exact solutions become practically indistinguishable. The agreement is further improved after powder integration, in the sense that the discrepancy between the two solutions becomes negligible at much shorter timescales (Fig. 2c), owing to cancellation of errors for individual crystallites. Thus, the solution of Eq. (14) can be used for an accelerated data analysis of R^2W experiments, and to gain additional insight into the R^2W dynamics. In particular, it is obvious from Eq. (14) that the R^2 transfer is rather insensitive to the deviation from the exact matching condition, as long as this deviation is much smaller than the ZQ relaxation rate, $\Delta \ll R$. Since carbonyl and methyl carbons span relatively narrow ranges of chemical shifts, ~10–15 ppm, it is possible to satisfy the condition $\Delta \ll R$ for many ^{13}CO–^{13}Cγ spin pairs simultaneously, and to recouple multiple ^{13}CO–^{13}Cγ contacts by simply shortening zero-quantum relaxation times. This can be achieved by reducing decoupling power during R^2 mixing. As will be discussed later, ZQ relaxation times observed experimentally in threonine, valine, and in the dipeptide NAcVL are all shorter than 1.5 ms. Thus, one expects that the R^2 bandwidth will be rather insensitive to the off-resonance term, as long as it is in the range of $\Delta \leqslant 0.5$ kHz. At the same time, the positions of Cα and most Cβ resonances are well separated from methyl peaks, so they can be kept significantly off of the rotational resonance condition, excluding them from the spin dynamics. Eq. (14) should also hold very well for the cases of very short relaxation times. In particular, it should be applicable for the description of the proton-driven spin diffusion experiment.

In the case of the magnetization exchange experiments when the initial longitudinal magnetization is prepared in the ZQ state $\rho(0) = \langle Q_1(0)\rangle - \langle Q_2(0)\rangle = I_{iz} - S_{jz}$, the steady-state approximation gives

$$\langle Q_1(t) - Q_2(t)\rangle = \langle I_{iz} - S_{jz}\rangle = \exp(-2\Omega t). \tag{17}$$

For the on-resonance case, $\Delta = 0$, and for vanishingly small chemical shift anisotropies, Eq. (17) can be reduced to

$$\langle Q_1(t) - Q_2(t)\rangle = \langle I_z - S_z\rangle = \exp\left\{-\frac{|\omega_{ij}^{(2)}|^2}{R}t\right\}, \tag{18}$$

the result previously obtained by Levitt et al. [52].

2.3.4. Effects of CSA on the polarization transfer

The effects of chemical shift anisotropy on the R^2 magnetization exchange experiments have been extensively studied [42,52,54–56]. For instance, the presence of CSA results in high order ($n > 2$) rotational resonance. The effects of CSA on polarization transfer efficiency at and around the $n = 2$ condition, and the implications it may have on the accuracy of distance measurements have also been analyzed previously [42,54]. Although there is relatively small degree of uncertainty in the carbonyl chemical shift anisotropy strength, the relative orientation of the dipolar and CSA tensors is unknown, and can greatly alter polarization transfer efficiency [42,54]. In particular, if σ_{33} component of the CSA tensor is parallel to the internuclear dipolar vector, the polarization transfer efficiency can reach about 90% [54]. In the other extreme, when σ_{33} component of the CSA tensor is perpendicular to the internuclear vector, the polarization transfer will be significantly diminished. Ramachandran et al. have shown that the CSA tensor orientation must be explicitly taken into account to extract accurate distances from the R^2W experiment [42]. In general, if relative orientations of the dipolar and CSA tensors are not known, the omission of the CSA effects will result in systematic errors of ±0.5–0.6 Å. Although their analysis was applied to the case of long relaxation rates, it also holds well if ZQ relaxation times are short, as confirmed in our simulations (results not shown). In this work, the CSA orientation is explicitly taken into account in the simulations.

2.3.5. Multi-spin effects in a three-spin system

So far, we have completely ignored any multi-spin effects, i.e., a possibility that one carbonyl spin can be simultaneously coupled to more than one aliphatic spin, or more than two carbonyls interact with one aliphatic spin or a few of them at the same time. The effective Hamiltonian can be easily generalized for the case of a multiple spin system, and is given as

$$H = \sum_i \Delta_{Ii} I_{iz} + \sum_i \Delta_{Si} S_{iz} + \sum_{i,j} B_{ij}(I_i^+ S_j^- + I_i^- S_j^+) + \sum_{i<j} 2\pi J_{ij} S_{iz} S_{jz}. \quad (19)$$

As before, the first two terms account for the off-resonance effects, while the flip–flop terms cause transitions between pairs of states $|\ldots\alpha_i\ldots\beta_j\ldots\rangle \leftrightarrow |\ldots\beta_i\ldots\alpha_j\ldots\rangle$. These states are nearly degenerate near the $n = 2$ R^2 condition. The last term accounts for J-couplings between aliphatic spins.

In the following, we focus on the three-spin topology typical for C′–Cγ recoupling experiments, where spin 1 is coupled to spins 2 and 3, while spins 2 and 3 do not interact with each other. Although a simplification, this topology retains many features intrinsic to the multi-spin recoupling experiments. Adequate description of the polarization exchange processes in such a three-spin system requires consideration of 18 coherences if J-coupling is taken into account, and 9 coherences if J-coupling is neglected. These coherences, as well as the corresponding Liouvillian matrix are given in the Appendix.

Fig. 3 shows the result of a three-spin simulation as a function of ZQ relaxation, and compares it with a simulation for an isolated spin pair. No J-coupling is considered in this case. The geometry of this three-spin system is described in the figure caption. A significant reduction of the polarization transfer efficiency between weakly coupled spins 1 and 3 in the presence of strongly coupled spins 1 and 2 has been documented in the literature, and is a manifestation of the dipolar truncation effect [20,21]. For a single crystallite, the polarization transfer efficiency ratio between $I_1 \to S_2$ to $I_1 \to S_3$ is proportional to $(B_{12}/B_{13})^2$. This attenuation of the polarization transfer between weakly coupled spins is significantly reduced if the ZQ relaxation is present. The main result demonstrated in Fig. 3 is that as the ZQ relaxation decreases from 5 ms in (a) to 0.5 ms in (d), the difference between the two-spin simulations (black curves) and three-spin simulations (open circles) diminishes.

To quantify these effects, the three-spin curves were fit using the two-spin model. The results of the two-spin fittings (shown as dashed grey curves in Fig. 3) are $R_{\text{eff}} = 4.7$ Å in (a), $R_{\text{eff}} = 4.5$ Å in (b), $R_{\text{eff}} = 4.4$ Å in (c), and $R_{\text{eff}} = 4.3$ Å in (d). These effective distances should be compared with the "true" distance of 4 Å, and serve as an estimate for a systematic uncertainty caused by the omission of multi-spin processes.

It is obvious that the ZQ relaxation, or more fundamentally the residual coupling to the proton bath plays an important role in the multi-spin R^2 polarization transfer dynamics. The multi-spin effects are reduced in the presence of short relaxation, and this corresponds well to our experimental situation (the extracted ZQ relaxation times are on the order of 1.0–1.5 ms in most cases). In particular, an error made by using two-spin approximation to interpret three-spin data for typical three-spin topologies is within 10% for $T_2^{\text{ZQ}} \sim 1$ ms, and even smaller for shorter T_2^{ZQ}.

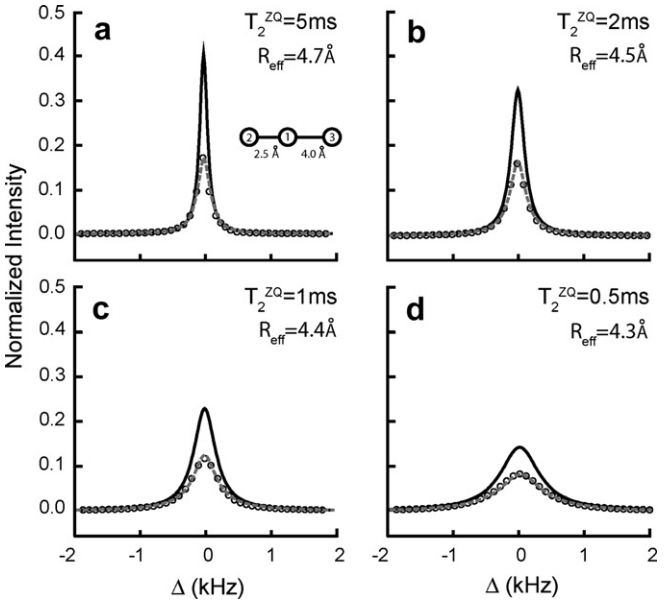

Fig. 3. R^2W simulations in a three-spin system. We consider a linear three-spin system where spin 1 is coupled to spins 2 and 3 as depicted in (a). Spin 1 resonates at zero frequency, while spins 2 and 3 have the same shift of 20 kHz. The R^2W curves were simulated in the vicinity of $n = 2$ resonance condition, and are shown as a function of deviation from the exact resonance, i.e., $\Delta = \delta - 2\nu_r$, where δ is the difference in isotropic chemical shifts between the coupled spins. The internuclear distances were $R_{12} = 2.5$ Å and $R_{13} = 4$ Å. The R^2 mixing time was chosen to be 40 ms. The zero-quantum relaxation times were as indicated in the figures. The signal intensity of the remote spin 3 is represented by open circles. The black curves represent R^2W signals for the same internuclear distance ($R_{13} = 4$ Å), but for a two spin model. The dashed grey curves represent the two-spin best fit to the three-spin solution. The best fit distances R_{eff} and the T_2^{ZQ} relaxation times extracted from the best (two-spin) fit were as follows: $R_{\text{eff}} = 4.7$ Å, $T_2^{\text{ZQ}} = 1.7$ ms in (a), $R_{\text{eff}} = 4.5$ Å, $T_2^{\text{ZQ}} = 1.2$ ms in (b), $R_{\text{eff}} = 4.4$ Å, $T_2^{\text{ZQ}} = 0.7$ ms in (c), and $R_{\text{eff}} = 4.3$ Å, $T_2^{\text{ZQ}} = 0.4$ ms in (d).

Additional simulations demonstrate that the aliphatic J-couplings ($J \sim 35$ Hz was considered) generally attenuate polarization transfer for long $T_2^{\text{ZQ}} > 5$ ms, but have negligible effect for short $T_2^{\text{ZQ}} \sim 1$ ms observed in this work (results not shown).

2.3.6. Simulations and data fitting

The two-spin simulations were performed using analytical expression of Eq. (14). Three-spin systems were solved accurately by the numerical diagonalization of the Eqs. (13), using average Liouvillian given in Appendix. In all cases, the dynamic phases resulting from the CSA were evaluated according to [55]:

$$\Phi_\Delta^{(ij)}(t) = \sum_{\substack{m=-2 \\ m\neq 0}}^{2} \frac{\omega_{Ii}^{(m)} - \omega_{Sj}^{(m)}}{im\omega_r}(e^{im\omega_r t} - 1), \quad (20)$$

The contribution from the dipolar and CSA interactions can be expressed in a single term [52]:

$$\tilde{\omega}_d^{ij}(t) = \omega_d^{(ij)}(t) \cdot e^{-i\Phi_\Delta^{(ij)}(t)} \quad (21)$$

It is necessary to find the second Fourier coefficient $\tilde{\omega}_d^{ij}$ that corresponds to the $n = 2$ R^2 condition. This coefficient was found numerically by calculating

$$B_{ij}^{(2)} = \frac{1}{\tau_r} \int_0^{\tau_r} \tilde{\omega}_d^{ij}(t) \cdot e^{-i2\omega_r t} dt, \quad (22)$$

and its absolute value $B_{ij} = |B_{ij}^{(2)}|$ was used to construct the Hamiltonian matrix.

All distances were extracted using an analytical solution of Eq. (14) for a two-spin model. One of the main advantages of the rotational resonance width method is that the interpretation of data does not require prior knowledge of the T_2^{ZQ} relaxation, and both internuclear distance and T_2^{ZQ} can be extracted unambiguously from the analysis of the recoupling resonance shape [40]. Thus a grid of R^2W curves was simulated for a range of internuclear distances and ZQ relaxation parameters, to which the experimental data were fit. The root-mean-square deviation (RMSD) between the experiment and simulated data was used as a test of the goodness of fit. The distance and ZQ relaxation parameter that yielded the lowest RMSD were taken to be the correct values. The R^2W curve was simulated for the best fit values and perturbed by randomly generated, normally distributed noise with a mean of zero and a standard deviation equal to the minimum RMSD of the original fit. The perturbed curve was refit to find the new distance and relaxation values. The Monte Carlo fitting was repeated ten thousand times, generating a histogram of parameter values. The interval in which 95% of the ten thousand points were able to be fit to was taken to be 95% confidence interval of the internuclear distance.

3. Experimental results and discussion

3.1. T_2^{ZQ} dependence on the decoupling power

Threonine was used to study the T_2^{ZQ} relaxation dependence on the decoupling power. We have run a set of 1D experiments (t_1 time is set to zero in the pulse sequence in Fig. 1) as a function of spinning frequency, and for different decoupling power levels. TPPM decoupling of ~79 kHz was used, as well as CW decoupling with power levels ranging from 100 to 45 KHz. A gradual widening of the R^2 condition was observed, reflecting the shortening of the ZQ relaxation times from 5.8 ms determined at 79 kHz TPPM decoupling, to ~1.1 ms at 45 kHz CW decoupling. For all decoupling power levels, the extracted $^{13}C'$–$^{13}C\gamma$ distances are in a good agreement with 3.03 Å determined by X-ray diffraction [57]. Further reduction of the decoupling power below 45 kHz reduces T_2^{ZQ} and broadens recoupling bandwidth, so the C′–Cα polarization transfer processes become visible. The presence of strong one-bond couplings in the spin dynamics is undesirable because it may complicate data interpretation and result in dipolar truncation effects. Thus the decoupling power was kept high enough to exclude alpha carbons from the polarization transfer. The recoupling bandwidth at the lowest decoupling power of 45 kHz can be estimated as ~0.5 kHz (twice the FWHM).

To check if T_2^{ZQ} relaxation times derived from the fitting of the R^2W curves correlate with SQ relaxation, the SQ line widths for $^{13}C'$ and $^{13}C\gamma$ were measured in natural abundance threonine under the decoupling conditions given in Fig. 4. We have found that the experimentally determined T_2^{ZQ} relaxation rates deviate from those estimated from the SQ line widths. For example, the line widths for $^{13}C'$ and $^{13}C\gamma$ were determined to be 19.0 and 20.5 Hz for 79 kHz TPPM decoupling, and 26.4 and 28.2 Hz for 45 CW decoupling. The corresponding T_2^{ZQ} relaxation parameters calculated from the SQ linewidths according to $1/T_2^{ZQ} = 1/2\pi(\Delta_{CO}^{1/2} + \Delta_{C\gamma}^{1/2})$ [58] are 4.0 ms and 2.9 ms for TPPM and CW decoupling, respectively.

U–^{15}N,^{13}C–Valine represents more complicated system consisting of at least three spins. Methyl resonances are well separated from methylene and alpha resonances, and it is possible to selectively recouple the dipolar interactions between carbonyl and methyl carbons. Again, a one-dimensional version of the experiment depicted in Fig. 1 was conducted as a function of spinning frequency for a series of decoupling powers. Significant broadening of the R^2 recoupling bandwidth was observed at reduced decoupling. Fig. 5 shows experimental R^2W curves at high decoupling (79 kHz TPPM) and low decoupling (CW, 45 kHz) powers. The overlap is minimal at high decoupling power in Fig. 5a, and one may expect that the V′–Vγ1 and V′–Vγ2 spin pairs will behave as independent two-spin systems. The best fit parameters are in a close agreement with the X-ray structure of valine that gives 3.88 Å and 2.99 Å for V′–Vγ1 and V′–Vγ2, respectively. The best fit relaxation is 2.2 ms, somewhat short compared to the threonine data in Fig. 4, where $T_2^{ZQ} \sim 5.8$ ms was observed under similar experimental conditions. This apparent shortening

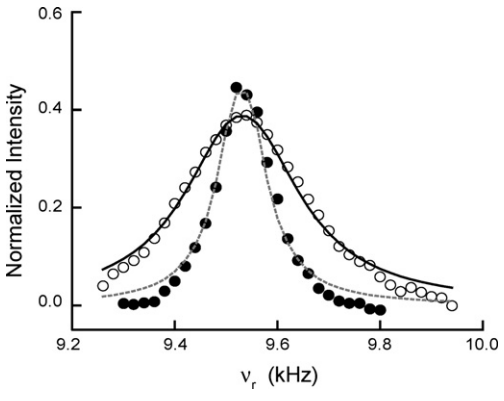

Fig. 4. R^2W curves of $T\gamma$ in threonine measured at different decoupling conditions. Solid circles represent signal intensities measured at TPPM decoupling of 79 kHz, and open circles are intensities measured at low CW decoupling power of ~45 kHz. Solid black and dashed grey curves represent best fit curves. Black curve corresponds to $R = 3$ Å, $T_2^{ZQ} = 5.8$ ms, and the dashed grey curve is $R = 2.95$ Å, $T_2^{ZQ} = 1.1$ ms. R^2W mixing time was 30 ms in both experiments.

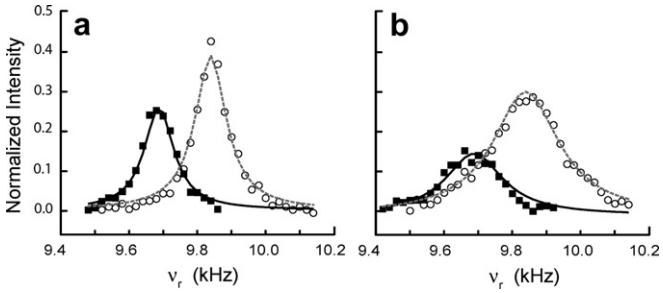

Fig. 5. R^2W curves of Vγ1 and Vγ2 in valine measured at different decoupling conditions. Solid squares represent experimentally measured intensities of Vγ1, and open circles represent signal intensities of Vγ2. R^2W measurements in (a) were conducted at TPPM decoupling of 79 kHz, and in (b)—at low power CW decoupling of 45 kHz. The best fit curves shown in figures were simulated with the following parameters: in (a) $R = 4$ Å, $T_2^{ZQ} = 2.2$ ms for Vγ1, $R = 3.4$ Å, $T_2^{ZQ} = 2.6$ ms for Vγ2. In (b) $R = 4$ Å, $T_2^{ZQ} = 1$ ms for Vγ1, $R = 3.2$ Å, $T_2^{ZQ} = 1$ ms for Vγ2. R^2W mixing time was 30 ms in both experiments.

of the relaxation time can be attributed to the residual multi-spin effects. Indeed attempting to fit three-spin systems with a two-spin simulation, as shown in Fig. 3, always yielded shorter relaxation times.

The reduction of the decoupling power broadens V′–Vγ1 and V′–Vγ2 resonances, and makes them strongly overlap, as shown in Fig. 5b. Similar to the effect observed in the experiments on threonine, the recoupling bandwidth can be roughly estimated as 0.4–0.5 kHz (twice the FWHM). Despite the overlap of V′–Vγ1 and V′–Vγ2 resonances, each of the R^2W curves can still be fit using two-spin approximation, and the extracted distances agree well with the X-ray data.

3.2. HBR^2 distance measurements in N-Ac-VL

Full 3D dipolar-chemical shift correlation experiments were conducted in the sample of N-Ac-Val-Leu, using pulse sequence in Fig. 1. The decoupling during R^2 mixing was again set to ~45 kHz, which results in the broadening of the R^2 recoupling conditions as discussed before. This decoupling power was the lowest possible level without reintroducing the C′–Cα interactions.

Fig. 6 shows a representative 2D spectrum taken at a spinning frequency of 9.6 kHz. At this spinning frequency, the $n = 2$ R^2 condition is nearly satisfied for V′–Vγ1 (exact matching at $\nu_R = 9.577$ kHz) and for L′–Lδ1 (exact matching at $\nu_R = 9.632$ kHz), and the corresponding cross peaks are at their maximum intensities. However, other resonances are also recoupled. In particular, V′–Vγ2 peak ($R = 2.97$ Å) is very intense despite the fact that it is ~0.46 kHz off (exact match is at $\nu_R = 9.832$ kHz). Even relatively weak interactions such as L′–Vγ2 dipolar coupling ($R = 4.54$ Å) are recoupled, despite that the chemical shift difference between L′ and Vγ2 resonances is off by as much as 0.8 kHz. Clearly, the reduction of the decoupling power allows for a significant increase in the recoupling bandwidth. Furthermore, the internuclear distances can be

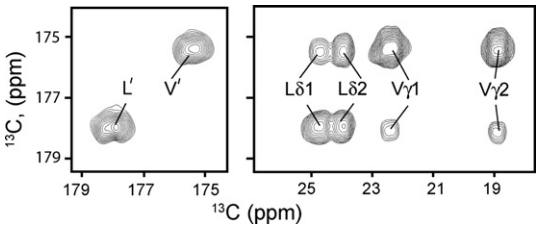

Fig. 6. Representative two-dimensional spectrum from the ^{13}C–^{13}C band selective R^2W experiment in *N*-Acetyl[U–^{13}C,^{15}N]L-Val-L-Leu obtained on 500 MHz spectrometer and at a spinning frequency of 9.6 kHz. The mixing time of 40 ms was used. All carbonyl–methyl side chain cross peaks are seen in the spectra, demonstrating increased bandwidth of the HBR^2.

extracted accurately using a simple two-spin model described above. Chemical shift anisotropy strengths and orientations for carbon atoms were taken from Ramachandran et al. and used in the simulations [42]. Typical R^2W curve for L′–Lδ1 and the best fit are shown in Fig. 7a. The peak intensities are referenced with respect to the sum of all peaks occurring at a given carbonyl frequency. This normalization is equivalent to the normalization with respect to the carbonyl intensity at zero mixing, provided that the T_1 relaxation is long on the scale of R^2 mixing, an assumption usually well justified. Sideband intensities are also taken into account for normalization.

A total of 11 distances were measured in this dipeptide. Overall, a good agreement with X-ray structure was obtained as evident from Fig. 7c and Table 1, with excep-

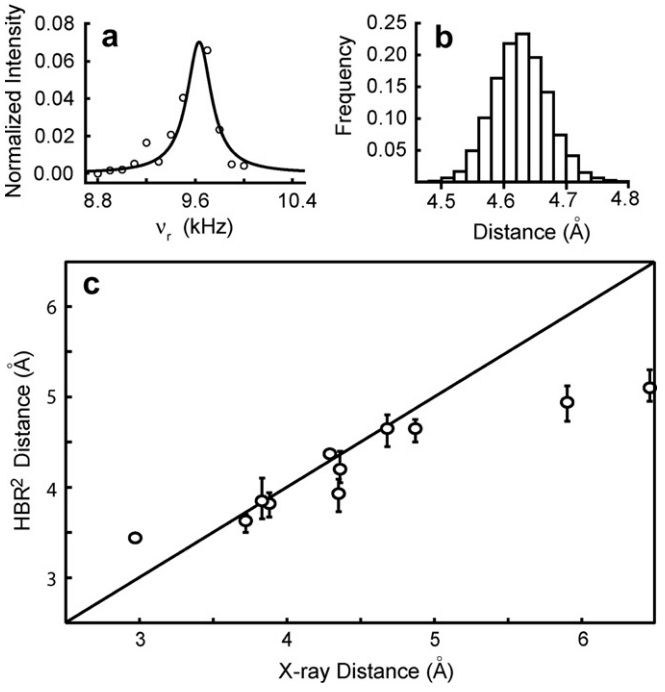

Fig. 7. (a) Comparison between experimentally determined R^2W curve for L′–Lδ1, open circles, and data simulated for the best fit internuclear distance and zero-quantum relaxation, solid black curve. The best fit curve was simulated with $R = 4.64$ Å, and $T_2^{ZQ} = 0.7$ ms. (b) Ten thousand iterations of Monte-Carlo fitting of L′–Lδ1, resulting in a 95% confidence interval of 4.54–4.70 Å for the internuclear distance. (c) Comparison of internuclear distances determined by HBR^2 and X-ray diffraction.

Table 1
Internuclear distances measured in N-Ac[U-^{13}C,^{15}N]L-Val-L-Leu by HBR^2 and X-ray diffraction

Atoms		^{13}C–^{13}C distance (Å)	
		HBR^2	X-ray
V′	Vγ2	3.44 (3.38–3.49)	2.97
	Vγ1	3.82 (3.67–3.94)	3.88
	Lδ1	4.37 (4.32–4.40)	4.29
	Lδ2	4.94 (4.73–5.12)	5.90
	Lγ	3.93 (3.73–4.09)	4.35
	Lb	3.63 (3.51–3.72)	3.72
L′	Vγ2	4.20 (4.05–4.40)	4.36
	Vγ1	5.12 (4.98–5.35)	6.46
	Lδ1	4.64(4.45–4.80)	4.87
	Lδ2	4.64(4.54–4.70)	4.68
	Lγ	3.85(3.67–4.08)	3.83

HBR^2 distances are given with a 95% confidence interval.

tion of V′–Lδ2 and L′–Vγ1 distances, which are clearly underestimated. Similar effects were observed in previous studies [41,59,60]. The explanation suggested in a number of previous publications was that these deviations could have been caused by the presence of residual intermolecular effects. The confidence intervals only account for random errors that result from experimental noise and the small thermal motions of the atoms but they fail to deal systematic errors such as using the two-spin simulation to fit data from a multi-spin system.

Although the side chain motions may have significant effects on the distance measurements discussed in this publication, the side chain molecular dynamics effects are relatively small in NAcVL. This is evident from the small B-factors (<7 Å^2) as determined by the X-ray studies [47]. The motions are probably limited to small librational motions of the atoms due to the close crystal packing, and it is reasonable to assume that any dynamic effects can be ignored in the extraction of internuclear distances in NAcVL. In proteins, however, special attention should be paid to the questions of motional averaging.

4. Conclusion

We have presented 3D band selective R^2 experiments, which are a straightforward expansion of the previously published R^2W method. The reduction of the decoupling power broadens the width of the rotational resonance, making the experiment band selective.

Apart from making R^2 band selective, the reduction of decoupling and shortening of the ZQ relaxation times seem to reduce the multi-spin effects permitting the application of a simple two-spin analysis to multi-spin data. We show that a simple analytical expression can be used to analyze data, and that the distances can still be determined with relatively high accuracy. The experiments have been demonstrated in NAcVL peptide where eleven intra- and inter-residue distances in a range between 2.9 and 6 Å were measured. The experiments were conducted at moderate spinning frequencies around $n = 2$ R^2 condition.

We expect the HBR^2 experiments conducted at moderate-field strengths (500 MHz) in this work to be applicable to structural measurements in non-crystalline biological solids, such as membrane proteins and insoluble peptide aggregates. Further extension of this simple method to proteins is under development in our lab, and will be presented in the forthcoming publication. It remains to be seen whether this methodology will be applicable at high magnetic fields. For instance, at 900 MHz carbonyl-aliphatic side chain $n = 2$ R^2 recoupling will require spinning frequencies on the order of 18 kHz. The broadening of rotational resonance condition under reduced decoupling observed in this work is homogeneous in nature, and will be less dependent on the radio-frequency power at high spinning frequencies.

Acknowledgments

This research was supported by the University of Guelph (start-up funds to V.L.), Natural Science and Engineering Research Council of Canada (Grant No. RG298480-04 to V.L), Canada Foundation for Innovation and Ontario Innovation Trust. V.L. holds Canada Research Chair Tier II in biophysics, and is a recipient of an Early Researcher Award. We would also like to thank one of the anonymous reviewers for useful comments.

Appendix A

The three-spin system where spin I_1(carbonyl) interacts with two aliphatic spins S_2 and S_3, and S_2 and S_3 are J-coupled, is described by the effective Hamiltonian

$$H = \Delta_1 I_{1z} + \Delta_2 S_{2z} + \Delta_3 S_{3z} + B_{12}(I_1^+ S_2^- + I_1^- S_2^+) + B_{13}(I_1^+ S_3^- + I_1^- S_3^+) + 2\pi J_{23} S_{2z} S_{3z} \quad \text{(A1)}$$

and can be conveniently represented in the basis set of 18 normalized operators:

$$\begin{aligned}
&Q_1 = 1/\sqrt{2} I_{1z}, \quad Q_2 = 1/\sqrt{2} S_{2z}, \quad Q_3 = 1/\sqrt{2} S_{3z},\\
&Q_4 = 1/2(I_1^+ S_2^- + I_1^- S_2^+), \quad Q_5 = -\mathrm{i}/2(I_1^+ S_2^- - I_1^- S_2^+),\\
&Q_6 = 1/2(I_1^+ S_3^- + S_1^- S_3^+), \quad Q_7 = -\mathrm{i}/2(I_1^+ S_3^- - S_1^- S_3^+),\\
&Q_8 = I_{1z}(S_2^+ S_3^- + S_2^- S_3^+), \quad Q_9 = -\mathrm{i} I_{1z}(S_2^+ S_3^- - S_2^- S_3^+),\\
&Q_{10} = S_{3z}(I_1^+ S_2^- + I_1^+ S_2^-), \quad Q_{11} = -\mathrm{i} S_{3z}(I_1^+ S_2^- - I_1^+ S_2^-),\\
&Q_{12} = S_{2z}(I_1^+ S_3^- + I_1^+ S_3^-), \quad Q_{13} = -\mathrm{i} S_{2z}(I_1^+ S_3^- - I_1^+ S_3^-)\\
&Q_{14} = 1/2(S_3^+ S_3^- - S_2^+ S_2^-), \quad Q_{15} = -\mathrm{i}/2(S_2^+ S_3^- - S_2^- S_3^+)\\
&Q_{16} = \sqrt{2} I_{1z} S_{2z}, \quad Q_{17} = \sqrt{2} S_{2z} S_{3z}, \quad Q_{18} = \sqrt{2} I_{1z} S_{3z}
\end{aligned} \quad \text{(A2)}$$

In this basis, the three-spin effective Liouvillian $\hat{L} = -\mathrm{i}\hat{\hat{H}} - \Gamma$ becomes

$$\hat{L} = \begin{pmatrix} \hat{L}_{11} & \hat{L}_{12} \\ -\hat{L}_{12}^T & \hat{L}_{22} \end{pmatrix} \quad \text{(A3)}$$

$$\hat{L}_{11} = \begin{pmatrix} & Q_1 & Q_2 & Q_3 & Q_4 & Q_5 & Q_6 & Q_7 & Q_8 & Q_9 \\ Q_1 & & & & & \sqrt{2}B_{12} & & \sqrt{2}B_{13} & & \\ Q_2 & & & & & -\sqrt{2}B_{12} & & & & \\ Q_3 & & & & & & & -\sqrt{2}B_{13} & & \\ Q_4 & & & & -R & -(\Delta_1-\Delta_2) & & & & -B_{13} \\ Q_5 & -\sqrt{2}B_{12} & \sqrt{2}B_{12} & & (\Delta_1-\Delta_2) & -R & & & -B_{13} & \\ Q_6 & & & & & & -R & -(\Delta_1-\Delta_3) & & B_{12} \\ Q_7 & -\sqrt{2}B_{13} & & \sqrt{2}B_{13} & & & (\Delta_1-\Delta_3) & -R & -B_{12} & \\ Q_8 & & & & & B_{13} & & B_{12} & -R & -(\Delta_2-\Delta_3) \\ Q_9 & & & & B_{13} & & -B_{12} & & (\Delta_2-\Delta_3) & -R \end{pmatrix} \tag{A4}$$

$$\hat{L}_{22} = \begin{pmatrix} & Q_{10} & Q_{11} & Q_{12} & Q_{13} & Q_{14} & Q_{15} & Q_{16} & Q_{17} & Q_{18} \\ Q_{10} & -R & -(\Delta_1-\Delta_2) & & & & -B_{13} & & & \\ Q_{11} & (\Delta_1-\Delta_2) & -R & & & -B_{13} & & & \sqrt{2}B_{12} & -\sqrt{2}B_{12} \\ Q_{12} & & & -R & -(\Delta_1-\Delta_3) & & B_{12} & & & \\ Q_{13} & & & (\Delta_1-\Delta_3) & -R & -B_{12} & & -\sqrt{2}B_{12} & \sqrt{2}B_{12} & \\ Q_{14} & & B_{13} & & B_{12} & -R & -(\Delta_2-\Delta_3) & & -B_{13} & \\ Q_{15} & B_{13} & & -B_{12} & & (\Delta_2-\Delta_3) & -R & & & \\ Q_{16} & & & & \sqrt{2}B_{13} & & & & & \\ Q_{17} & & -\sqrt{2}B_{12} & & -\sqrt{2}B_{13} & & & & & \\ Q_{18} & & \sqrt{2}B_{12} & & & & & & & \end{pmatrix} \tag{A5}$$

$$\hat{L}_{12} = \begin{pmatrix} & Q_{10} & Q_{11} & Q_{12} & Q_{13} & Q_{14} & Q_{15} & Q_{16} & Q_{17} & Q_{18} \\ Q_1 & & & & & & & & & \\ Q_2 & & & & & & & & & \\ Q_3 & & & & & & & & & \\ Q_4 & & \pi J_{23} & & & & & & & \\ Q_5 & -\pi J_{23} & & & & & & & & \\ Q_6 & & & & \pi J_{23} & & & & & \\ Q_7 & & & -\pi J_{23} & & & & & & \\ Q_8 & & & & & & & & & \\ Q_9 & & & & & & & & & \end{pmatrix} \tag{A6}$$

In the matrices above, only non-zero elements are shown. We also assumed the same decay rate for zero-quantum and double-quantum coherences that can be formed between spins 1 and 2, 1 and 3, and 2 and 3. If J-coupling is neglected, the matrix becomes block-diagonal, and only the first nine differential equations are important in determining the time evolution of populations $\langle S_{1z}\rangle$, $\langle S_{2z}\rangle$, $\langle S_{3z}\rangle$. These equations can be solved either by numerical diagonalization of the Liouvillian, or through finding a steady-state analytical solution to this system, assuming that the sum $\langle S_{1z}\rangle + \langle S_{2z}\rangle + \langle S_{3z}\rangle$ stays constant.

References

[1] E.R. Andrew, A. Bradbury, E. R.G, Nuclear magnetic resonance spectra from a crystal rotated at high speed, Nature 182 (1958) 1659.

[2] J. Pauli, M. Baldus, B. van Rossum, H. de Groot, H. Oschkinat, Backbone and side-chain C-13 and N-15 signal assignments of the alpha-spectrin SH3 domain by magic angle spinning solid-state NMR at 17.6 tesla, Chembiochem 2 (2001) 272–281.

[3] C.M. Rienstra, L. Tucker-Kellogg, C.P. Jaroniec, M. Hohwy, B. Reif, M.T. McMahon, B. Tidor, T. Lozano-Perez, R.G. Griffin, De novo determination of peptide structure with solid-state magic-angle spinning NMR spectroscopy, Proceedings of the National Academy of Sciences of the United States of America 99 (2002) 10260–10265.

[4] F. Castellani, B. van Rossum, A. Diehl, M. Schubert, K. Rehbein, H. Oschkinat, Structure of a protein determined by solid-state magic-angle-spinning NMR spectroscopy, Nature 420 (2002) 98–102.
[5] C.P. Jaroniec, C.E. MacPhee, N.S. Astrof, C.M. Dobson, R.G. Griffin, Molecular conformation of a peptide fragment of transthyretin in an amyloid fibril, Proceedings of the National Academy of Sciences of the United States of America 99 (2002) 16748–16753.
[6] C.P. Jaroniec, C.E. MacPhee, V.S. Bajaj, M.T. McMahon, C.M. Dobson, R.G. Griffin, High-resolution molecular structure of a peptide in an amyloid fibril determined by magic angle spinning NMR spectroscopy, Proceedings of the National Academy of Sciences of the United States of America 101 (2004) 711–716.
[7] S. Luca, J.F. White, A.K. Sohal, D.V. Filippov, J.H. van Boom, R. Grisshammer, M. Baldus, The conformation of neurotensin bound to its G protein-coupled receptor, Proceedings of the National Academy of Sciences of the United States of America 100 (2003) 10706–10711.
[8] A. Lange, K. Giller, S. Hornig, M.F. Martin-Eauclaire, O. Pongs, S. Becker, M. Baldus, Toxin-induced conformational changes in a potassium channel revealed by solid-state NMR, Nature 440 (2006) 959–962.
[9] A.T. Petkova, Y. Ishii, J.J. Balbach, O.N. Antzutkin, R.D. Leapman, F. Delaglio, R. Tycko, A structural model for Alzheimer's beta-amyloid fibrils based on experimental constraints from solid state NMR, Proceedings of the National Academy of Sciences of the United States of America 99 (2002) 16742–16747.
[10] H. Heise, W. Hoyer, S. Becker, O.C. Andronesi, D. Riedel, M. Baldus, Molecular-level secondary structure, polymorphism, and dynamics of full-length alpha-synuclein fibrils studied by solid-state NMR, Proceedings of the National Academy of Sciences of the United States of America 102 (2005) 15871–15876.
[11] S. Luca, D.V. Filippov, J.H. van Boom, H. Oschkinat, H.J.M. de Groot, M. Baldus, Secondary chemical shifts in immobilized peptides and proteins: a qualitative basis for structure refinement under Magic Angle Spinning, Journal of Biomolecular Nmr 20 (2001) 325–331.
[12] D.S. Wishart, B.D. Sykes, The C-13 chemical-shift index—a simple method for the identification of protein secondary structure using C-13 chemical-shift data, Journal of Biomolecular Nmr 4 (1994) 171–180.
[13] S. Spera, A. Bax, Empirical correlation between protein backbone conformation and C-Alpha and C-Beta C-13 nuclear-magnetic-resonance chemical-shifts, Journal of the American Chemical Society 113 (1991) 5490–5492.
[14] R.G. Griffin, Dipolar recoupling in MAS spectra of biological solids, Nature Structural Biology 5 (1998) 508–512.
[15] F. Creuzet, A. Mcdermott, R. Gebhard, K. Vanderhoef, M.B. Spijkerassink, J. Herzfeld, J. Lugtenburg, M.H. Levitt, R.G. Griffin, Determination of membrane-protein structure by rotational resonance Nmr—Bacteriorhodopsin, Science 251 (1991) 783–786.
[16] L.K. Thompson, A.E. Mcdermott, J. Raap, C.M. Vanderwielen, J. Lugtenburg, J. Herzfeld, R.G. Griffin, Rotational resonance nmr-study of the active-site structure in bacteriorhodopsin—conformation of the Schiff-base linkage, Biochemistry 31 (1992) 7931–7938.
[17] L.M. McDowell, M.S. Lee, R.A. McKay, K.S. Anderson, J. Schaefer, Intersubunit communication in tryptophan synthase by carbon-13 and fluorine-19 REDOR NMR, Biochemistry 35 (1996) 3328–3334.
[18] L.M. McDowell, A. Schmidt, E.R. Cohen, D.R. Studelska, J. Schaefer, Structural constraints on the ternary complex of 5-enolpyruvylshikimate-3-phosphate synthase from rotational-echo double-resonance NMR, Journal of Molecular Biology 256 (1996) 160–171.
[19] D.P. Weliky, A.E. Bennett, A. Zvi, J. Anglister, P.J. Steinbach, R. Tycko, Solid-state NMR evidence for an antibody-dependent conformation of the V3 loop of HIV-1 gp120, Nature Structural Biology 6 (1999) 141–145.
[20] M. Hohwy, C.M. Rienstra, C.P. Jaroniec, R.G. Griffin, Fivefold symmetric homonuclear dipolar recoupling in rotating solids: application to double quantum spectroscopy, Journal of Chemical Physics 110 (1999) 7983–7992.
[21] M. Hohwy, C.M. Rienstra, R.G. Griffin, Band-selective homonuclear dipolar recoupling in rotating solids, Journal of Chemical Physics 117 (2002) 4973–4987.
[22] V. Ladizhansky, E. Vinogradov, B.J. van Rossum, H.J.M. de Groot, S. Vega, Multiple-spin effects in fast magic angle spinning Lee-Goldburg cross-polarization experiments in uniformly labeled compounds, Journal of Chemical Physics 118 (2003) 5547–5557.
[23] T.G. Oas, R.G. Griffin, M.H. Levitt, Rotary resonance recoupling of dipolar interactions in solid-state nuclear magnetic-resonance spectroscopy, Journal of Chemical Physics 89 (1988) 692–695.
[24] N.C. Nielsen, H. Bildsoe, H.J. Jakobsen, M.H. Levitt, Double-quantum homonuclear rotary resonance—efficient dipolar recovery in magic-angle-spinning nuclear-magnetic-resonance, Journal of Chemical Physics 101 (1994) 1805–1812.
[25] K. Takegoshi, S. Nakamura, T. Terao, C-13–H-1 dipolar-driven C-13–C-13 recoupling without C-13 rf irradiation in nuclear magnetic resonance of rotating solids, Journal of Chemical Physics 118 (2003) 2325–2341.
[26] C.R. Morcombe, V. Gaponenko, R.A. Byrd, K.W. Zilm, Diluting abundant spins by isotope edited radio frequency field assisted diffusion, Journal of the American Chemical Society 126 (2004) 7196–7197.
[27] A. Grommek, B.H. Meier, M. Ernst, Distance information from proton-driven spin diffusion under MAS, Chemical Physics Letters 427 (2006) 404–409.
[28] S.G. Zech, A.J. Wand, A.E. McDermott, Protein structure determination by high-resolution solid-state NMR spectroscopy: application to microcrystalline ubiquitin, Journal of the American Chemical Society 127 (2005) 8618–8626.
[29] D.P. Raleigh, M.H. Levitt, R.G. Griffin, Rotational resonance in solid-state Nmr, Chemical Physics Letters 146 (1988) 71–76.
[30] K. Takegoshi, K. Nomura, T. Terao, Rotational resonance in the tilted rotating-frame, Chemical Physics Letters 232 (1995) 424–428.
[31] K. Takegoshi, K. Nomura, T. Terao, Selective homonuclear polarization transfer in the tilted rotating frame under magic angle spinning in solids, Journal of Magnetic Resonance 127 (1997) 206–216.
[32] P.R. Costa, B.Q. Sun, R.G. Griffin, Rotational resonance tickling: accurate internuclear distance measurement in solids, Journal of the American Chemical Society 119 (1997) 10821–10830.
[33] A.K. Paravastu, R. Tycko, Frequency-selective homonuclear dipolar recoupling in solid state NMR, Journal of Chemical Physics 124 (2006) 194303.
[34] E.R. Andrew, A. Bradbury, E. R.G., W. V.T, Nuclear cross relaxation induced by specimen rotation, Physics Letters 4 (1963) 99–100.
[35] E.R. Andrew, A. Bradbury, E. R.G, W. V.T, Resonant rotational broadening of nuclear magnetic resonance spectra, Physics Letters 21 (1966) 505–506.
[36] M.G. Colombo, B.H. Meier, R.R. Ernst, Rotor-driven spin diffusion in natural-abundance C-13 spin systems, Chemical Physics Letters 146 (1988) 189–196.
[37] P.T.F. Williamson, A. Verhoeven, M. Ernst, B.H. Meier, Determination of internuclear distances in uniformly labeled molecules by rotational-resonance solid-state NMR, Journal of the American Chemical Society 125 (2003) 2718–2722.
[38] A. Verhoeven, P.T.F. Williamson, H. Zimmermann, M. Ernst, B.H. Meier, Rotational-resonance distance measurements in multi-spin systems, Journal of Magnetic Resonance 168 (2004) 314–326.
[39] A.T. Petkova, R. Tycko, Rotational resonance in uniformly C-13-labeled solids: effects on high-resolution magic-angle spinning NMR spectra and applications in structural studies of biomolecular systems, Journal of Magnetic Resonance 168 (2004) 137–146.
[40] P.R. Costa, B.Q. Sun, R.G. Griffin, Rotational resonance NMR: separation of dipolar coupling and zero quantum relaxation, Journal of Magnetic Resonance 164 (2003) 92–103.
[41] R. Ramachandran, V. Ladizhansky, V.S. Bajaj, R.G. Griffin, C-13–C-13 rotational resonance width distance measurements in uniformly C-13-labeled peptides, Journal of the American Chemical Society 125 (2003) 15623–15629.

[42] R. Ramachandran, J.R. Lewandowski, P.C.A. van der Wel, R.G. Griffin, Multipole-multimode Floquet theory of rotational resonance width experiments: C-13–C-13 distance measurements in uniformly labeled-solids, Journal of Chemical Physics 124 (2006).
[43] D.K. Sodickson, M.H. Levitt, S. Vega, R.G. Griffin, Broad-band dipolar recoupling in the nuclear-magnetic-resonance of rotating solids, Journal of Chemical Physics 98 (1993) 6742–6748.
[44] A.E. Bennett, J.H. Ok, R.G. Griffin, S. Vega, Chemical-shift correlation spectroscopy in rotating solids—radio frequency-driven dipolar recoupling and longitudinal exchange, Journal of Chemical Physics 96 (1992) 8624–8627.
[45] G. Goobes, G.J. Boender, S. Vega, Spinning-frequency-dependent narrowband RF-driven dipolar recoupling, Journal of Magnetic Resonance 146 (2000) 204–219.
[46] G. Goobes, S. Vega, Improved narrowband dipolar recoupling for homonuclear distance measurements in rotating solids, Journal of Magnetic Resonance 154 (2002) 236–251.
[47] P.J. Carroll, P.L. Stewart, S.J. Opella, Structures of 2 Model Peptides—*N*-acetyl-D,L-Valine and *N*-acetyl-L-Valyl-L-Leucine, Acta Crystallographica Section C-Crystal Structure Communications 46 (1990) 243–246.
[48] A. Pines, M.G. Gibby, J.S. Waugh, Proton-enhanced Nmr of dilute spins in solids, Journal of Chemical Physics 59 (1973) 569–590.
[49] S.R. Hartmann, E.L. Hahn, Nuclear double resonance in the rotating frame, Physical Review 128 (1962) 2042–2053.
[50] A.E. Bennett, C.M. Rienstra, M. Auger, K.V. Lakshmi, R.G. Griffin, Heteronuclear decoupling in rotating solids, Journal of Chemical Physics 103 (1995) 6951–6958.
[51] F. Delaglio, S. Grzesiek, G.W. Vuister, G. Zhu, J. Pfeifer, A. Bax, Nmrpipe—a multidimensional spectral processing system based on Unix pipes, Journal of Biomolecular Nmr 6 (1995) 277–293.
[52] M.H. Levitt, D.P. Raleigh, F. Creuzet, R.G. Griffin, Theory and simulations of homonuclear spin pair systems in rotating solids, Journal of Chemical Physics 92 (1990) 6347–6364.
[53] R.R. Ernst, G. Bodenhausen, A. Wokaun, Principles of Nuclear Magnetic Resonance in One and Two Dimensions, Clarendon Press, Oxford, 1991.
[54] P.R. Costa, D.A. Kocisko, B.Q. Sun, P.T. Lansbury, R.G. Griffin, Determination of peptide amide configuration in a model amyloid fibril by solid-state NMR, Journal of the American Chemical Society 119 (1997) 10487–10493.
[55] T. Karlsson, M.H. Levitt, Longitudinal rotational resonance echoes in solid state nuclear magnetic resonance: investigation of zero quantum spin dynamics, Journal of Chemical Physics 109 (1998) 5493–5507.
[56] M. Helmle, Y.K. Lee, P.J.E. Verdegem, X. Feng, T. Karlsson, J. Lugtenburg, H.J.M. de Groot, M.H. Levitt, Anomalous rotational resonance spectra in magic-angle spinning NMR, Journal of Magnetic Resonance 140 (1999) 379–403.
[57] J. Janczak, D. Zobel, P. Luger, l-Threonine at 12 K, Acta Crystallographica Section C 53 (1997) 1901–1904.
[58] A. Kubo, C.A. Mcdowell, Spectral spin diffusion in polycrystalline solids under magic-angle spinning, Journal of the Chemical Society-Faraday Transactions I 84 (1988) 3713–3730.
[59] C.P. Jaroniec, B.A. Tounge, J. Herzfeld, R.G. Griffin, Frequency selective heteronuclear dipolar recoupling in rotating solids: accurate C-13–N-15 distance measurements in uniformly C-13, N-15-labeled peptides, Journal of the American Chemical Society 123 (2001) 3507–3519.
[60] V. Ladizhansky, R.G. Griffin, Band-selective carbonyl to aliphatic side chain C-13–C-13 distance measurements in U–C-13,N-15-labeled solid peptides by magic angle spinning NMR, Journal of the American Chemical Society 126 (2004) 948–958.